Coupled oscillator systems of cultured cardiac myocytes: Fluctuation and scaling properties

Mitsuru Yoneyama
Research Institute for Electronic Science, Hokkaido University, Sapporo 060-0812, Japan
and Mitsubishi Chemical Group, Science and Technology Research Center, Inc., Yokohama 227-8502, Japan

Koichi Kawahara
Research Institute for Electronic Science, Hokkaido University, Sapporo 060-0812, Japan
(Received 28 February 2004; revised manuscript received 20 April 2004; published 11 August 2004)

Isolated and cultured neonatal cardiac myocytes exhibit autonomous rhythmic contraction, and their dynamics vary dramatically depending on the extent of mutual coupling among individual myocytes. We study the temporal changes of interbeat interval series in aggregated systems of spontaneously beating cultured neonatal rat cardiac myocytes and observe a rich variety of complex, nonlinear features such as frequent alternations, bistability, and periodic spikes. Fluctuation analysis of the interval series reveals that there occurs a transition in scaling behavior from persistent correlations to antipersistent correlations as the coupling develops with incubation time. Additionally, we perform computer simulations using interacting Bonhoeffer-van der Pol oscillators to understand the effects of coupling on the fluctuation dynamics of each constituent oscillator. We find that the formation of strong and heterogeneous coupling among the oscillators is a key factor to yield the complexity in the interval series as well as in the scaling behavior.

DOI: 10.1103/PhysRevE.70.021904 PACS number(s): 87.18.−h, 05.40.−a, 89.75.Da

I. INTRODUCTION

Living organisms display various types of biological rhythms such as heartbeat, respiration, sleep-wake cycle, and locomotor activity. In most cases these rhythms are endogenous, i.e., driven by a spontaneously oscillating pacemaker element or a network of many interacting elements. In the network system each constituent element, which has an intrinsic property as a self-sustaining oscillator in an isolated state, often exhibits collective phenomena due to mutual coupling. A typical example of such a system is the sinoatrial (SA) node, a small region in the right atrium of the heart, composed of thousands of pacemaker cells. When isolated enzymatically from the SA node, the cells show independent oscillations with different frequencies. In spite of this behavior, a coherent electrical wave is generated in a periodic fashion within the SA node, which spreads throughout the heart and controls its beating rate.

In general, biological rhythms are not strictly regular, but entail complex fluctuations that reflect their underlying control mechanisms [1]. Numerous attempts have been made to explore the function and origin of these complex processes, with special attention paid to human cardiac dynamics owing to its physiological and clinical importance [2,3]. Mathematical analyses so far have revealed that cardiac rhythms as well as other physiological rhythms arise from nonlinear, stochastic processes, thus producing such unique features as chaos, fractal dynamics, long-range correlations, and $1/f^{\beta}$ noise [1]. Kobayashi and Musha were the first to report that the power spectrum of heart rate variability (HRV) possesses a strong $1/f$ component over a wide frequency range [4]. Since then, HRV has been repeatedly confirmed to have a fractal temporal structure [5,6]. Recently, a new challenge has been posed to this understanding by Ivanov *et al.* who found that HRV patterns of healthy individuals are much more complex, showing multifractal scaling [7]. All these findings make it increasingly clear that stochasticity or noise which brings about the fluctuations, either inherent in biological systems or from a fluctuating environment, is an integral part of the underlying dynamics [8]. However, still very little is known about the exact mechanism and functional significance of such fluctuations, particularly in spatially extended systems of many coupled elements.

In a previous paper, we investigated the contraction rhythm of spontaneously beating cultured cardiac myocytes in order to clarify the relationship between its fluctuation and possible interactions among the myocytes [9]. The coefficient of variation of contraction intervals increased in the early periods of incubation, and then decreased in a monotonic way. Furthermore, the contraction rhythms of interacting myocytes showed mutual entrainment (synchronization) late in culture. We concluded that these temporal changes were caused by an increase in coupling strength among the myocytes with culture time. Here we present experimental and simulation studies on the fluctuation and correlation properties of interbeat intervals (IBIs) in coupled systems of cardiac myocytes. We report that the scaling patterns of IBI fluctuations show a dramatic dependence on culture time possibly due to day-to-day changes in the degree of mutual coupling.

II. METHODS

Isolated and cultured cardiac myocytes of neonatal rats were prepared, and their rhythmic contraction was monitored by a video-image recording method as described previously [9]. Images of spontaneously beating myocytes were recorded once a day. The obtained image (about $420 \times 320\ \mu m^2$) contained more than 10 cardiac myocytes. A small area (20×20 pixels) of a myocyte showing considerable changes in brightness with contraction was selected

from the image, and the video signal was digitized to an 8-bit number per every video frame (30 frames/s) for 3 min. A reference frame was arbitrarily selected and cross correlograms were calculated between pixels of the reference frame and those of other frames, which represent temporal variations of brightness in the selected area corresponding to the contraction rhythm of the myocyte. Cubic splines were fit to the cross correlogram in each series of data from each day for the detection of upward or downward peak positions, and IBIs were calculated from the intervals between successive peaks.

The correlation properties of the IBI series were investigated utilizing detrended fluctuation analysis (DFA) [10]. DFA calculates the root-mean-square fluctuation function $F(n)$ of a time series around local trends for different window sizes (time scales) n, which gives a power law relation $F(n) \sim n^{\alpha}$ in the presence of scaling. Although the main advantage of the DFA method is that it allows the accurate estimation of long-range correlations embedded in noisy, nonstationary time series, it is also powerful in quantifying short-range or intermediate-range temporal properties by the scaling exponent α, i.e., whether the time series is anticorrelated (antipersistent, $\alpha < 0.5$), uncorrelated (random, $\alpha = 0.5$), or correlated (persistent, $\alpha > 0.5$).

In order to model the contraction rhythm of a single cardiac myocyte, a pair of first-order differential equations known as the Bonhoeffer-van der Pol (BVP) oscillator was adopted [9,11],

$$\dot{x} = c(x - x^3/3 + y + z),$$

$$\dot{y} = -(x + by - a)/c, \tag{1}$$

where x denotes the membrane potential, y the slower recovery process, z the external stimulus applied to the oscillator, and a, b, c are constants. With appropriate values of the constants, the BVP oscillator shows stable limit cycles corresponding to the physiological properties of cardiac pacemaker cells. In the present paper, we set $a = b = z = 0$ without loss of generality, which gives the original van der Pol equation. The stochastic nature of the oscillation intervals of the BVP model was introduced by setting $c = c_0 + c_1 n(t)$ [9], where $n(t)$ stands for normally distributed random numbers with a noise power of 0.005.

For numerical simulations of aggregated cardiac myocytes that are electrically and/or mechanically interacting with each other, a network of N coupled BVP oscillators was used. The model takes the form

$$\dot{x}_i = c_i[x_i - x_i^3/3 + (y_i + y_i^{\text{out}})], \quad y_i^{\text{out}} = \sum_j \gamma_{ij} y_j,$$

$$\dot{y}_i = -x_i/c_i, i = 1, \ldots, N, \tag{2}$$

where y_i^{out} represents the interaction term with coupling strength γ_{ij}. Here, the constant c_i has different values among the oscillators, and is defined as follows:

$$c_i = c_{0i} + c_{1i} n(t),$$

$$c_{0i} = 5.0 + 0.5(2i - N - 1)/(N - 1),$$

$$c_{1i} = 2.0. \tag{3}$$

This guarantees each BVP oscillator in the coupled system to have its intrinsic rhythmicity, reflecting the individuality of actual cardiac myocytes. In Eq. (2), the coupling term is not the widely used diffusive type; it is introduced as a modification of the slow variable (y_i) in the equation of motion for the fast variable (x_i). This approach is based on the application of a generalized receptor scheme that has been proposed recently by Nagano to provide a general mathematical framework for explaining various synchronization phenomena in biological systems [12]. In short, the generalized receptor scheme treats one of two variables x_i and y_i constituting a limit cycle oscillation as the density of a virtual diffusible chemical (ligand) and the other as the activity of a virtual receptor to catch the ligand. Each receptor in an individual oscillator works as a converter of external stimuli from other oscillators into internal stimuli, which leads to efficient synchronization among the entire oscillators. In our case [Eq. (2)], x_i, y_i, and γ_{ij} correspond to receptorlike activity, ligandlike density, and the sensitivity of the receptor, respectively, and the summation Σ_j covers all oscillators including a self-term ($j = i$). The biological meaning of this correspondence and the advantages of the generalized receptor scheme over the conventional diffusion scheme will be discussed later.

Calculations of the BVP oscillator network were performed with the variable-step Dormand–Prince formula loaded in the MATLAB/Simulink system (The MathWorks, Inc.). The oscillation intervals of the BVP model were evaluated from intervals between downward peaks of $x(t)$, then divided by 10 (in time unit) to adjust time scale, and their scaling properties were analyzed by the DFA method. We checked that similar results were obtained using other solvers for computer simulation much more suited for dealing with stiff problems.

III. RESULTS

A. IBI fluctuations of cardiac myocytes

The video recording of cardiac myocytes was started on the third day of culture when most myocytes began to show spontaneous contraction. We chose two myocytes (referred to as cell 1 and cell 2 hereafter) from the recorded image for continual observation of contraction rhythm. The two myocytes on the fourth day of culture were spatially separated, but on the 11th day they appeared to be fully connected with each other via other myocytes growing between them [9]. The IBI series of the two cells from the third to the 13th day of culture are displayed in Figs. 1(a) and 1(b). The data for cell 1 on the third day is not presented in Fig. 1(a) because the contraction rhythm showed only irregular, intermittent oscillations, from which it was very difficult to extract IBIs. It is seen that the two sequences of data follow almost identical time evolution: the IBI values of both cells have an overall tendency to decrease with incubation time, and there are many similar structures in the time series, for example, transient bursts occurring on the fourth day [indicated by arrows in Figs. 1(a) and 1(b)] and extremely large fluctuations on the fifth and sixth day. It was found in the previous

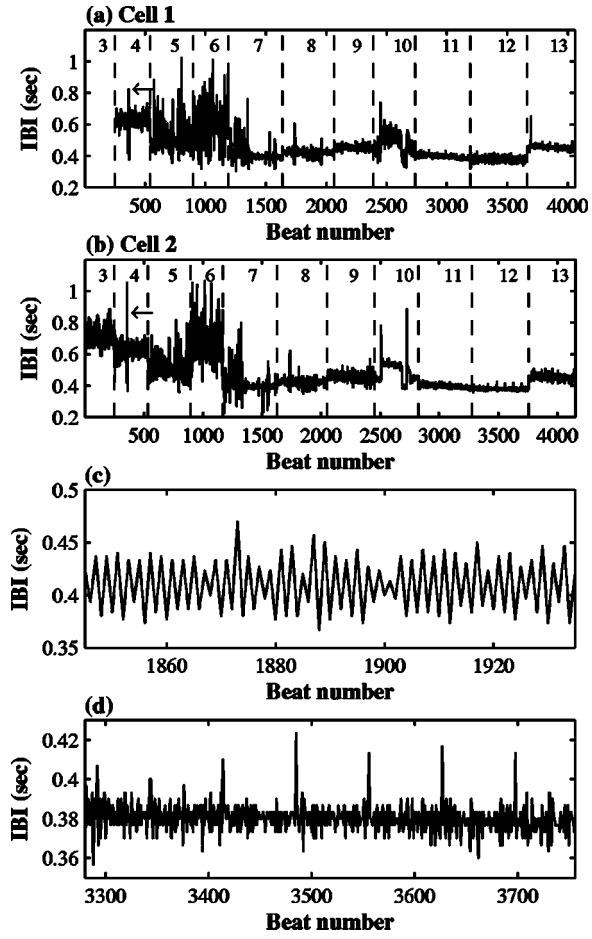

FIG. 1. Interbeat interval (IBI) series of two cardiac myocytes: (a) cell 1 and (b) cell 2. The signal is obtained by stitching together the IBI series for each culture day indicated by the numbers 3–13, whose boundaries are marked by dashed lines. The arrows indicate transient bursts almost simultaneously occurring in both series on the fourth day. (c) Enlargement of (a) record for day 8, showing rapid alternations. (d) Enlargement of (b) record for day 12, showing clear spikes with a period of about 70.

work that the two myocytes exhibited no noticeable synchronization of contraction before the seventh day of culture [9]. However, the remarkable similarity between the two time courses in the present case suggests that the cultured myocytes may exert a subtle influence upon one another from the start of the video recording.

In addition to the above observation, several complex but interesting features are noticed in the IBI series: (1) On the seventh day, large fluctuations seen at early stages suddenly disappear near a midpoint in the series. (2) On the eighth day, the IBI shows rapid alternations indicative of strong anticorrelated behavior around the middle portion in the series [Fig. 1(c)]. (3) On the 10th day, there emerges a kind of bistability: the IBI displays abrupt transitions back and forth between two states overlapped by a slight decreasing trend. (4) On the 12th day for cell 2 (and also on the 11th day for cell 1, although not clear to see), characteristic spikes are observed periodically [Fig. 1(d)]. The appearance of distinct anticorrelations in Fig. 1(c) results from the onset of a period doubling in the contraction rhythm as shown in Fig. 2. The

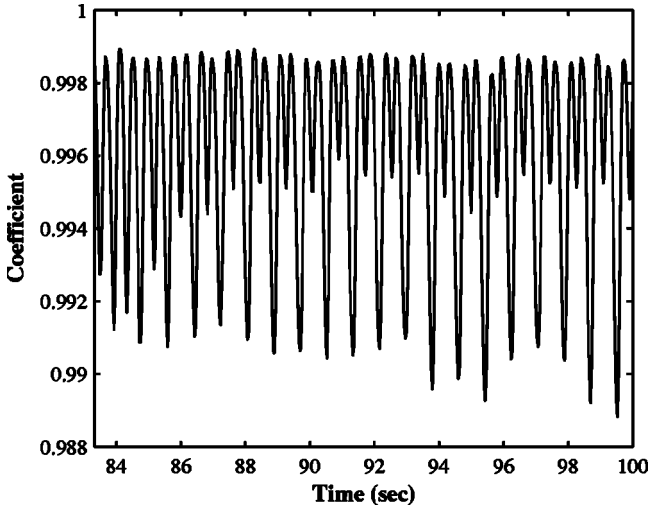

FIG. 2. Spontaneous beating of cell 1 on the eighth day of culture, showing the onset of period-doubling oscillation. The contraction rhythm of the myocyte is represented as the temporal change in the cross-correlation coefficient.

IBIs are derived from two consecutive peaks so that an interval measured from a lower peak to its succeeding higher peak gives a different value compared to that from a higher peak to its succeeding lower peak, thus producing the alternating temporal behavior.

These features are a clear indication that the oscillating dynamics of the cardiac myocytes are indeed governed by some highly nonlinear processes. The fact that the complex temporal behaviors are mostly observed after the seventh day of incubation, when the contraction rhythms of the two myocytes were found to achieve full synchronization in our previous finding [9], demonstrates that the underlying nonlinearity originates from large interactions among the myocytes.

For the analysis of correlation properties, we applied the first order DFA (using a polynomial fit of order 1 for a local trend) to each IBI series from each culture day after removing noisy points that are far away from its mean value. Since the series on the seventh day are composed of two segments with different local fluctuations, i.e., the first half with large fluctuations and the rest, the DFA method was applied separately to each of these two segments. Likewise, two sequences with and without rapid alternations were picked out from the series on the eighth day for separate analysis. For the 10th day data, which exhibit abrupt changes due to bistability, we examined only the segments that have a larger mean interval.

Figures 3(a)–3(d) illustrate the DFA profiles of the two myocytes. It is apparent that both the fluctuation function $[F(n)]$ and its differential function $[d\log 10F(n)/d\log 10n(=\alpha)]$ show drastic changes with time in culture, suggesting a strong dependence of the correlation behavior on the degree of coupling among the myocytes. In order to see this dependence more clearly, we focus on the scaling properties of the IBI records at small scales. The short-range scaling exponent was calculated in the range $0.6 \leqslant \log_{10} n \leqslant 0.8$ as a mean value of $d\log_{10} F(n)/d\log_{10} n$, and plotted as a function of incu-

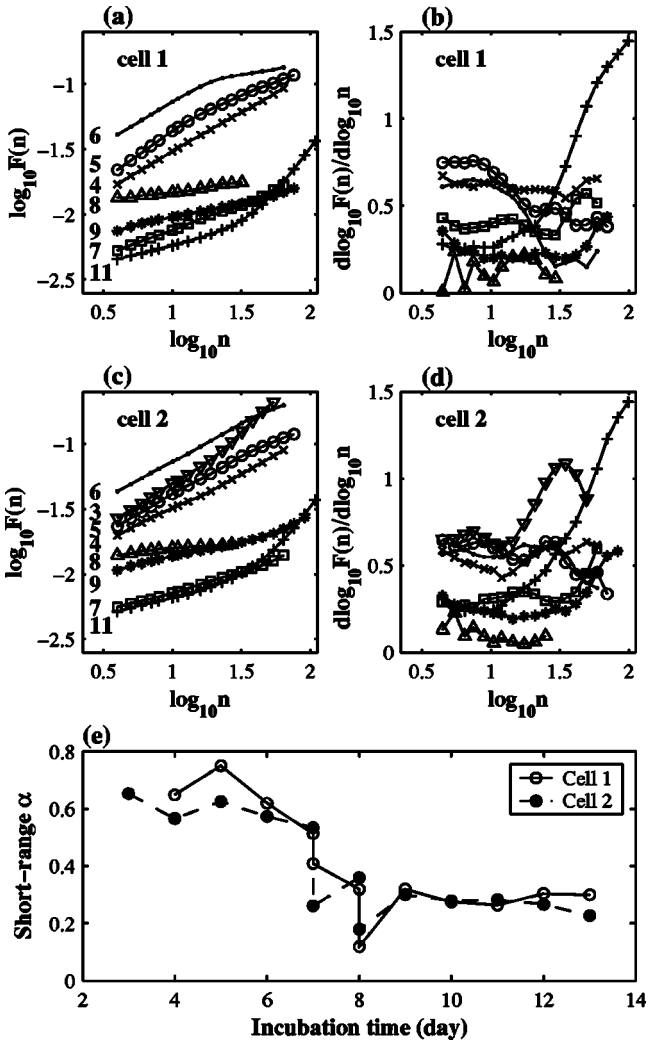

FIG. 3. Detrended fluctuation analysis (DFA) of the IBI series of two cardiac myocytes. Two segments with different fluctuation patterns were extracted from the IBI series on the seventh and eighth day of culture, and DFA was applied separately to each segment (see text). Fluctuation functions (a) and (c), and differential fluctuation functions (b) and (d) are shown for the following days of culture: day 3 (∇); day 4 (×); day 5 (○); day 6 (•); day 7 (□); day 8 (Δ); day 9 (*); day 11 (+). The culture days are represented by the numbers beside the plots in (a) and (c). For days 7 and 8, only the results for the segments with small fluctuations and with rapid alternations are displayed, respectively. The differential fluctuation function was obtained by calculating slopes between successive points in the fluctuation function. (e) Changes in the short-range scaling exponent with incubation time. A transition from correlated behavior ($\alpha > 0.5$) into anticorrelated behavior ($\alpha < 0.5$) occurs on the seventh day.

bation time [Fig. 3(e)]. For both cell 1 and cell 2, we note a characteristic transition on the seventh day, where there is a sudden change from persistent correlations ($\alpha > 0.5$) to antipersistent correlations ($\alpha < 0.5$). The loss of correlation (or rather, enhancement of anticorrelation) in the scaling behavior, since it occurs on the same seventh day as complete synchronization was found to occur in our previous study [9], is also considered to be a direct consequence of an increase in coupling strength among the myocytes.

Interestingly, before the seventh day when the two cells are not synchronous and therefore appear to have no strong interactions with each other, the short-range scaling exponent is well over 0.5, reaching as high as 0.75 for cell 1 on the fifth day. This may be easy to understand if it is assumed that the IBI fluctuations of an individual myocyte are already correlated in an isolated state and their correlation properties are more or less maintained in the presence of weak coupling with other myocytes. Such an assumption, however, has not yet been justified experimentally, so here we simply postulate that the dynamics of each noninteracting myocyte is characterized by uncorrelated randomness ($\alpha = 0.5$). Later, we will show by computer simulations that the scaling properties of an isolated myocyte with random behavior can be brought into persistent correlations ($\alpha > 0.5$) via the introduction of small interactions with other myocytes. On culture days 3 and 4, the correlations remain persistent even at long-time scales ($\log_{10} n > 1$) [Figs. 3(b) and 3(d)]. Most notable is the case of cell 2 on the third day, where there is a crossover to a more correlated regime with the scaling exponent $\alpha > 1$ around $\log_{10} n \approx 1.5$. In contrast, the DFA differential curves on days 5 and 6 exhibit a gradual downward trend at long-time scales, especially for cell 1, indicating that the IBI sequence behaves like either a periodic or a random signal at these scales.

After the seventh day, the short-range scaling exponent reduces to around 0.3 except on the eighth day when it takes a very small value ($\alpha < 0.2$), reflecting the highly antipersistent nature as we have seen in Fig. 1(c). Generally, when the DFA method is used to analyze a sinusoidal signal with period shorter than the minimum window size for calculation, a marked zigzag shape appears at small scales in the plot of differential fluctuation function. Such a pattern is clearly seen in the DFA results on the eighth day [Figs. 3(b) and 3(d)]. On the other hand, if a fluctuating signal contains as its dominant components some periodicity with periods longer than the minimum window size, its differential fluctuation function tends to be upward concave and the minimum regions are located around time scales corresponding to the periodicity. This is indeed what we observe to take place in the profiles after the ninth day [Figs. 3(b) and 3(d)], in which there is a shallow depression around $\log_{10} n \approx 1$, suggesting that the contraction dynamics of interacting myocytes are under the control of multimodal periodicity with periods centered at 10 (in beat number) or more.

It should be mentioned that these correlation properties are not an artifact produced by the cutout of noisy points prior to analysis. This type of data preprocessing is known to have a significant effect on the scaling properties of anticorrelated signals [13]. Before the seventh day, the IBI series is so noisy that the fraction of points removed from the original series becomes very large. Nevertheless, the cutting procedure is expected to have little influence on the scaling behavior of such signals with persistent correlations ($\alpha > 0.5$). We actually confirmed this by comparing the DFA profiles with and without preprocessing; the cutting procedure led to a vertical shift to smaller values of the fluctuation function, but

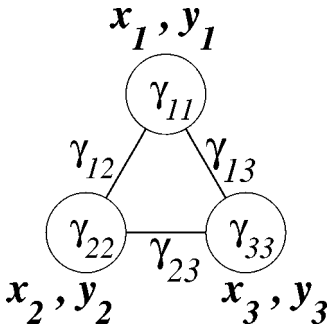

FIG. 4. A diagram representing the configuration of three BVP oscillators with coupling strength γ_{ij}. Variables x_i and $y_i (i=1,2,3)$ denote the membrane potential and recovery variable, respectively. The coupling strength inside each circle represents the self-term (γ_{ii}), and that by each side connecting two circles represents the mutual term.

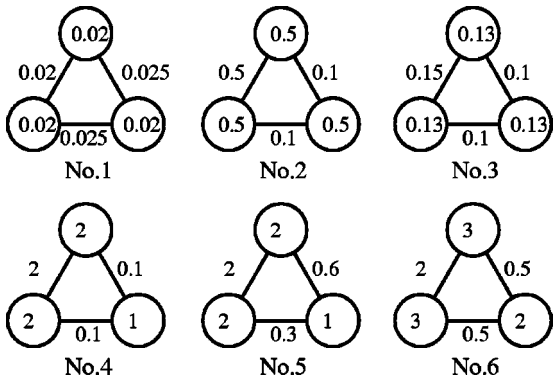

FIG. 5. Examples of coupling strengths used in the simulation of BVP model. Number 1 corresponds to the observed IBI series on day 4; No. 2 to day 5; No. 3 to day 6; No. 4 to the less fluctuating part on day 7; No. 5 to the rapidly alternating part on day 8; No. 6 to day 9.

no remarkable change in the differential fluctuation function. After the seventh day, the IBI series becomes much less noisy, and therefore the effect of preprocessing is thought to be also insignificant. We notice for particular IBI series, e.g., on the 11th day, that the scaling exponent exhibits a characteristic crossover to strong positive correlations ($\alpha > 1$) at long-time scales. Obviously, this crossover cannot be explained by the cutting procedure, as its primary effect on anticorrelated signals is to increase the scaling exponent close to 0.5 at most [13]. Rather, the crossover results from some polynomial trends contained in the series because using higher-order DFA was found to reduce the scaling exponent at these long-time scales effectively.

B. Simulation with BVP model

With a view to modeling the observed fluctuation properties, we performed computer simulations of three BVP oscillators [$N=3$ in Eq. (2)] for various coupling strengths. Our strategy is to capture the major experimental observations, the complex IBI fluctuations and their scaling patterns in particular, by assigning a different set of coupling strengths $\gamma_{ij} (1 \leqslant i, j \leqslant 3)$ to myocytes on each culture day while holding other parameters fixed. The coupling strengths thus assigned are unchanged throughout the calculation period for the corresponding culture day. It is not intended here to exactly reproduce all the quantitative features, e.g., mean IBI values, although this could be done through appropriate adjustment in such parameters as a, b, and c in Eq. (1). The configuration of the coupled system is schematically illustrated as a triangular diagram in Fig. 4, in which a symmetrical mutual coupling is assumed ($\gamma_{ij} = \gamma_{ji}$). Typical values of coupling selected for simulation are indicated in Fig. 5 (Nos. 1–6), and calculated oscillation interval series and their DFA results are summarized in Fig. 6 together with the corresponding experimental results for the purpose of comparison.

In our simulation, the mean oscillation interval is found to decrease almost monotonically for all oscillators as any one of the nine coupling strengths increases. Therefore, the global trend towards smaller IBI values with incubation time [Figs. 1(a) and 1(b)] can be reproduced by simply increasing the coupling strengths. However, in order to elucidate the time course from the fifth to the sixth day where the mean IBI is larger on the later culture day [Fig. 6(d)], we must use lower values of coupling for No. 3 compared to No. 2 [Figs. 5 and 6(a)]. Then, the calculated time dependence agrees quite well with the IBI series except for the series on the ninth day [Figs. 6(a) and 6(d)]. It may be possible to simulate this local inverse tendency observed on the ninth day as well as on the 13th day with appropriate choices of the coupling strengths. But at such late stages of culture it is likely that a role played by some physiological changes in individual myocytes rather than decreased mutual interactions becomes much more prominent in generating the inverse tendency.

Most of the observed complex features, i.e., the rapid alternations on the eighth day and the bistable character on the 10th day, are successfully reproduced with simulation as illustrated in Figs. 7(a) and 7(b). The occurrence of spikes with a period of about 70 on the 12th day is also reproducible but with comparatively large values of coupling [Fig. 7(c)]; as a consequence the calculated mean oscillation interval becomes extremely small, whereas in the experiment the mean IBI changes little with time in culture after the seventh day. The only case where our theoretical strategy fails is the sudden disappearance of large fluctuations on the seventh day, which cannot be simulated unless the coupling strengths or other parameters are altered accordingly in the middle of the calculation period.

In the absence of interaction among the three oscillators ($\gamma_{ij}=0$), the fluctuation function for each oscillator behaves as $F(n) \sim n^{0.5}$ at small and intermediate scales (data not shown). This seems natural considering that the dynamics of an independent oscillator is under the control of uncorrelated randomness inherent in the constant c_i [Eq. (3)]. Surprisingly, when positive weak couplings are introduced among the uncorrelated oscillators, the fluctuations begin to possess persistent correlations with the short-range scaling exponent $\alpha > 0.5$ [see the plots for Nos. 2 and 3 in Figs. 6(b) and 6(c)]. The dominance of correlated behavior at small scales is in good agreement with the experiment, and its mechanism can be understood as follows. For specific values of coupling, especially when all the mutual coupling strengths exceed 0.1,

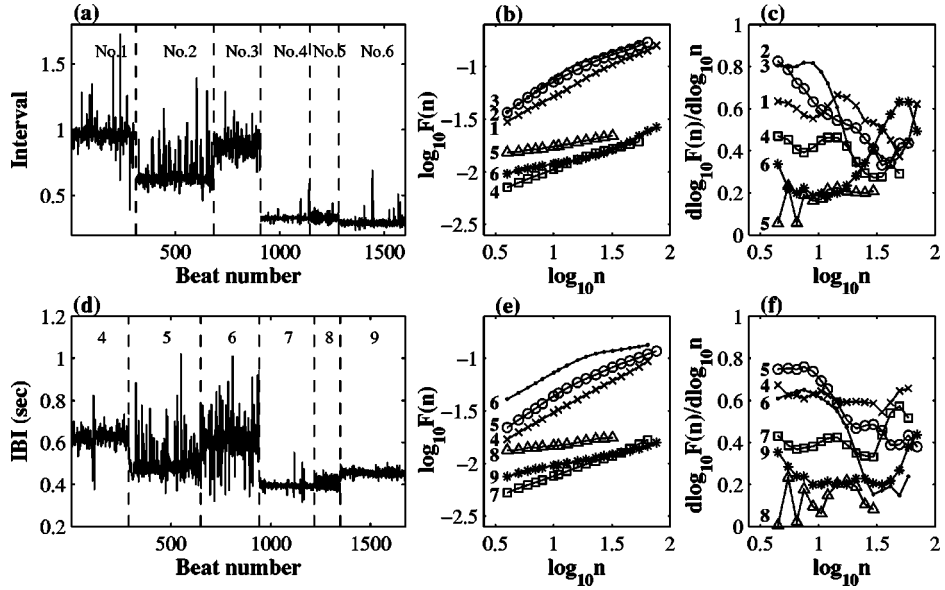

FIG. 6. A comparison between simulation and observation. (a) Simulated temporal changes in the oscillation interval of x_1. Each number corresponds to the configuration number in Fig. 5. (b), (c) Simulated fluctuation functions and differential fluctuation functions: No. 1 (×); No. 2 (○); No. 3 (•); No. 4 (□); No. 5 (Δ); No. 6 (*). The numbers beside the plots represent the configuration numbers. (d) Observed temporal changes in the IBI of cell 1. The numbers represent the days of culture. For days 7 and 8, only the results on the segments with small fluctuations and with rapid alternations are displayed, respectively. (e), (f) Experimental fluctuation functions and differential fluctuation functions: day 4 (×); day 5 (○); day 6 (•); day 7 (□); day 8 (Δ); day 9 (*). The numbers beside the plots represent the days of culture. Simulation and experimental results agree well.

the oscillation interval tends to switch between two or more discrete levels with time. As an example, a comparison between the IBI series on the fifth day and the calculated series for No. 2 is made in Fig. 8. Both series have similar time dependence, with occasional spiking from a lower baseline to higher interval values. As this example illustrates, the switching occurs as a series of rather broad spikes, which is the reason why the fluctuations of the oscillation interval exhibit persistent correlations at scales smaller than the width of the spike and weaker correlations at larger scales. Moreover, the temporal transitions between discrete levels turn out to be the primary cause for the large fluctuations in the IBI series observed on the fifth and sixth days [Figs. 1(a) and 1(b)].

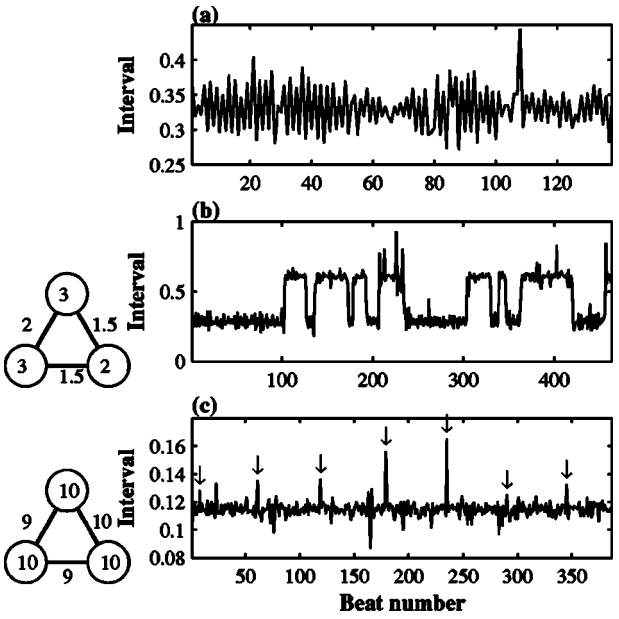

FIG. 7. Simulated temporal changes in the oscillation interval of x_1 showing (a) rapid alternations, (b) bistability, and (c) periodic spikes. (a) is an enlargement of Fig. 6(a) record for No. 5. The arrows in (c) indicate the positions of the spikes. Coupling strengths used for the calculation of (b) and (c) are illustrated as a diagram on the left-hand side of each time series.

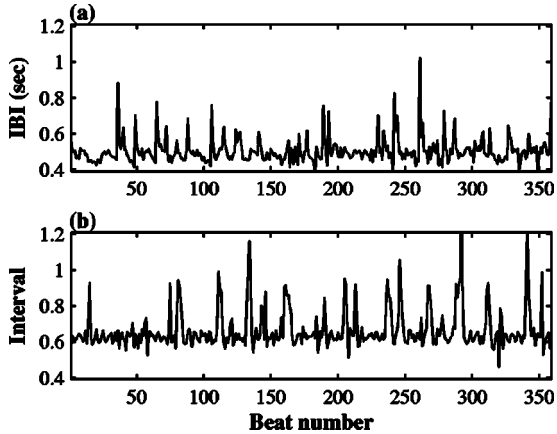

FIG. 8. A comparison between the IBI series of cell 1 on the fifth day of culture and simulated temporal changes in the oscillation interval x_1 for No. 2. Both plots are consistent with each other in that they show a similar train of broad spikes bursting from a fluctuating baseline.

As the coupling strengths are increased further, the scaling behavior undergoes a transition into antipersistent correlations ranging over almost all scales [Nos. 4–6 in Figs. 6(b) and 6(c)]. It is notable that the observed scaling patterns due to strong (multi)periodicity after the seventh day of culture, including the characteristic zigzag shape, are successfully simulated. In achieving $\alpha < 0.5$ for most of the window sizes, it is essential to allocate different values to different coupling terms (see Nos. 4–6 in Fig. 5). The same condition is also necessary to bring about the distinctive nonlinearity as seen in Fig. 7. A qualitative explanation for this requirement is that with common strengths for all coupling terms, the three oscillators are in such a complete synchronization as to behave like a single oscillator and hence their fluctuation dynamics are determined mainly by the white noise in the constant c_i, while if the nine coupling strengths are not all identical, some of the oscillators are a little asynchronous with one another and a complex interplay between such out-of-synch pairs can produce a multiperiodic modulation on their temporal fluctuations.

IV. DISCUSSION

All these results demonstrate that a number of experimental observations concerning the fluctuation dynamics of cardiac myocytes have been reproduced in a systematic way by calculations of BVP coupled oscillators. Increasing the number of oscillators from three to five led to similar results but with undesirable complications because of undue parameters that have to be changed, so the current three-element system offers the simplest sufficient model to explain the essence of our experimental findings.

We focused on the effect of varying coupling strength with other parameters fixed throughout the simulation analysis. This strategy revealed that the presence of strong and nonuniform coupling among the oscillators is required to yield distinct anticorrelations in the oscillation interval fluctuations. It is expected that the same mechanism may be also working in real myocyte networks. Of course, the validity of this argument must be checked by careful comparison of theoretical coupling values with measurable ones. In addition, we should consider the possibility of some electrophysiological changes within the myocytes to play a significant role in generating the observed fluctuation behavior. Since experimental information on these issues is currently lacking, detailed studies will be necessary to quantify the degree of coupling on each culture day and distinguish its contribution from that of other physiological changes. We have just started a few attempts in this line and have obtained some preliminary results. First, in order to clarify the effect of intracellular physiology, we aimed at characterizing the fluctuation dynamics of a single neonatal cardiac myocyte in a completely isolated state, which turned out to be unsuccessful; it seems that our neonatal cell cannot remain viable by itself and needs interactions with neighboring cells for its survival and growth. So next, we employed 12-doxyl stearic acid (DSA), a reversible blocker of gap junction channels, to produce an artificially uncoupled system from aggregated myocytes. The treatment of highly interacting myocytes with DSA was found to cause a change in their scaling behavior from strong anticorrelations ($\alpha < 0.2$) to uncorrelations ($\alpha \approx 0.5$), and also a drastic increase in IBI. This experimental evidence, although too limited to completely exclude the contribution of intracellular physiological changes, offers a strong support of our scenario that cardiac myocyte cells, whose IBI fluctuations are intrinsically uncorrelated, begin to show anticorrelations with time in culture due to the development of mutual coupling. More systematic research based on selective pharmacological blockade will help to separate intercellular and/or extracellular influences on myocytes from intracellular ones for each culture day, enabling us to understand the observed day-to-day changes in scaling behavior in a more quantitative way.

Our theoretical approach is an extension of the generalized receptor scheme recently developed by Nagano [12]. For simulating a network of interacting oscillators, diffusive coupling has been frequently employed and been proved quite effective. So, we compared the performance of both approaches by carrying out another set of calculations with the following equations:

$$\dot{x}_i = c_i\left[x_i - x_i^3/3 + y_i + \sum_j D_{ij}(x_j - x_i)\right], \quad D_{ij} = D_{ji},$$

$$\dot{y}_i = -x_i/c_i, \quad i = 1, \ldots, N, \tag{4}$$

where D_{ij} is the diffusive coupling strength. For three coupled oscillators ($N=3$), it was found that Eq. (4) gives signals whose short-range scaling exponent is around 0.5 and never less than 0.3 irrespective of the values for coupling. Therefore, the appearance of strong anticorrelations after the seventh day of culture could not be simulated with the diffusive-type model. Moreover, the mean oscillation interval obtained by Eq. (4) did not show great changes with increasing coupling strength. This is usually the case for coupling via diffusive exchange because the oscillation interval of fully synchronized oscillators tends to take an intermediate value among that of individual oscillators before synchronization. The observed mean IBI for cell 2 decreased from 0.7 s on day 3 to 0.4 s on day 7, corresponding to almost a 40% change, a difference unlikely to be explained using the diffusive-type model by variations in coupling strength in the absence of other physiological changes. In our cultured myocytes, the IBI often decreased with the development of mutual coupling (see the time evolutions of cell 1 and cell 2 in Fig. 1), although in rare cases we encountered an increasing trend with incubation time probably due to reduced cell viability. Simulating this temporal behavior was also beyond the performance of the diffusive-type model which actually claims that nearly half of the oscillators involved in the coupling should display increasing oscillation interval with increasing coupling strength. Moreover, other complex features such as bistability and periodic spikes could not be reproduced using Eq. (4). Therefore, our model in the present study has many advantages over the conventional diffusive-type model in elucidating the characteristic dynamics found in the IBI series of interacting myocytes.

Although the current ligand-receptor scheme can be regarded as a general mathematical framework to describe synchronization phenomena, it is important to discuss the biological meaning of this model. Intercellular gap junction channels generally provide the main pathway for intercellular communication among cardiac myocytes. The major gap junction protein in cardiac myocytes is connexin 43, which forms channels that are permeable to intracellular messengers such as Ca^{2+}, inositol (1,4,5)-triphosphate (IP3), ATP, and cAMP [14]. Additionally, a paracrine route, mediated by the diffusion of extracellular messengers such as ATP, can also operate in parallel with the direct cell-to-cell interaction via gap junction channels [15]. Thus, cardiac myocytes have two intercellular communication routes. Changes in the intracellular concentration of Ca^{2+} and IP3 associated with spontaneous rhythmic contraction of cardiac myocytes may affect neighboring cells through gap junction channels. For instance, IP3 transported from one cell to the other cells via gap junction may activate IP3 receptors of sarcoplasmic reticulum (SR). The activation of IP3 receptors results in Ca^{2+} release from the SR (IP3-induced Ca^{2+} release), and thus influences the contraction rhythm of the myocytes. In addition, cAMP diffusion through gap junction channels possibly affects the contraction rhythm in neighboring cardiac myocytes as well. Lader *et al.* recently reported in cultured neonatal rat myocytes that cAMP activates an ATP-permeable pathway, and then results in ATP release to extracellular spaces [16]. Cultured cardiac myocytes are known to express purinoceptors sensitive to ATP, so the increase in extracellular ATP may provide autocrine as well as paracrine influences on the contraction rhythm of cardiac myocytes. Based on this simplified picture, it is reasonable to speculate that the messengers such as IP3 and ATP correspond to virtual ligands, and their sensors such as IP3 receptors and purinoceptors correspond to virtual receptors in the ligand-receptor scheme. The inclusion of the self-term (γ_{ii}) in Eq. (2) is then justified because it can be interpreted as a mathematical description of the autocrine pathway. The mutual term ($\gamma_{ij}, i \neq j$) is thought to reflect the two intercellular communication routes, i.e., the direct interaction via gap junction and the paracrine route. Among them, the paracrine route mediated by the diffusion of extracellular messengers is probably responsible for intercellular communication at early stages of incubation (before the fourth day) when cultured cardiac myocytes are found to interact a little without any conspicuous physical contacts among one another. This schematic scenario, although speculative, should help in guiding future research as to intercellular communication among cultured cardiac myocytes and its relation to contraction rhythm dynamics.

Finally, it is informative to examine what will happen if we introduce negative values of coupling, at least from a purely mathematical viewpoint. The variable x_i in Eq. (2) has a stable limit cycle so long as the total contribution from the recovery variable y is positive in the equation of motion of x_i, which is roughly expressed by the condition $1+\Sigma_j \gamma_{ij} > 0$. Figure 9 exemplifies a case satisfying this condition with negative strengths for two mutual couplings. Remarkably, the oscillation fluctuations exhibit persistent correlations and the scaling exponent exceeds 1 at larger window sizes, which

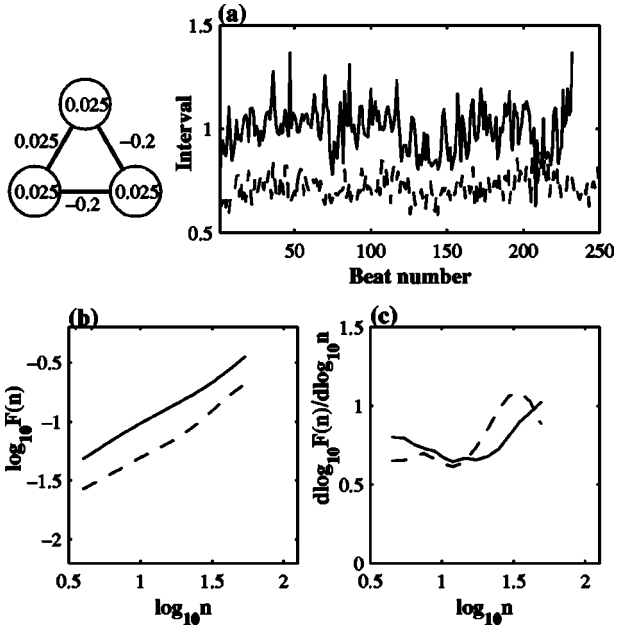

FIG. 9. An example of negative mutual coupling: (a) oscillation interval; (b) fluctuation function; (c) differential fluctuation function. Two mutual coupling strengths out of the three are set to negative values (−0.2) as shown in the diagram. Simulation results are indicated by solid lines, while dashed lines represent experimental results on the third day of culture for cell 2, both demonstrating strong memory effects ($\alpha > 1$) at large window sizes.

is in good accord with the experimental behavior on the third day [Fig. 3(d)]. This result is quite stimulating since we have not succeeded in simulating a crossover from a correlated regime at small scales to a more correlated regime at large scales when using only positive coupling strengths. The negative mutual coupling means that the virtual ligand from one unit of the coupled pair exerts an inhibitory effect on the virtual receptor of the other unit. It is possible that the same negative coupling may also play a key role in real aggregated myocytes at early stages of culture for producing strong memory effects ($\alpha > 1$) at long-time scales. Inhibitionlike effects are ubiquitous in physiological systems such as the chronotropic effect of ATP on mammalian cardiac pacemaker cells [17], but the existence of inhibitory interactions has not yet been identified experimentally among cultured neonatal cardiac myocytes. Therefore, thorough discussion on the significance of negative coupling should await further experimental studies.

V. CONCLUSION

In summary, we investigate fluctuation dynamics in IBI series of cultured neonatal rat cardiac myocytes and demonstrate a marked dependence of correlation properties on incubation time. The short-range scaling exponent decreases almost monotonically as the culture period increases, showing a transition from correlated to anticorrelated states, which is accompanied by the emergence of highly nonlinear phenomena in IBI series such as rapid alternations, bistability, and periodic spikes. From simulation studies using

coupled BVP oscillators, we suggest the importance of strong and heterogeneous coupling among constituent elements in reproducing the observed complex behaviors. Our model is intended to simulate the experimental fluctuation patterns on each culture day by adjusting coupling strengths while keeping other parameters constant throughout the calculation; it should not be treated as an ideal model to explain all the details in contraction dynamics of interacting cardiac myocytes. Nonetheless, we believe that the current scheme may contribute to uncovering hidden information on the mechanism and functional significance of biological fluctuations in spatially extended systems.

[1] L. Glass, Ann. Telecommun. **410**, 277 (2001).

[2] M. C. Teich, S. B. Lowen, B. M. Jost, K. Vibe-Rheymer, and C. Heneghan, in *Nonlinear Biomedical Signal Processing, Vol. II, Dynamic Analysis and Modeling*, edited by M. Akay (IEEE Press, New York, 2001).

[3] R. Fischer, M. Akay, P. Castiglioni, and M. Di Rienzo, Med. Biol. Eng. Comput. **41**, 543 (2003).

[4] M. Kobayashi and T. Musha, IEEE Trans. Biomed. Eng. **29**, 456 (1982).

[5] B. J. West and A. L. Goldberger, Am. Sci. **75**, 354 (1987).

[6] Y. Yamamoto and R. L. Hughson, Am. J. Physiol. **266**, R40 (1994).

[7] P. Ch. Ivanov, L. A. N. Amaral, A. L. Goldberger, S. Havlin, M. G. Rosenblum, Z. R. Struzik, and H. E. Stanley, Nature (London) **399**, 461 (1999).

[8] T. Kuusela, T. Shepherd, and J. Hietarinta, Phys. Rev. E **67**, 061904 (2003).

[9] Y. Yamauchi, A. Harada, and K. Kawahara, Biol. Cybern. **86**, 147 (2002).

[10] C. K. Peng, S. V. Buldyrev, S. Havlin, M. Simons, H. E. Stanley, and A. L. Goldberger, Phys. Rev. E **49**, 1685 (1994).

[11] R. FitzHugh, Biophys. J. **1**, 445 (1961).

[12] S. Nagano, Phys. Rev. E **67**, 056215 (2003).

[13] Z. Chen, P. Ch. Ivanov, K. Hu, and H. E. Stanley, Phys. Rev. E **65**, 041107 (2002).

[14] M. V. Bennett, L. C. Barrio, T. A. Bargiello, D. C. Spray, E. Hertzberg, and J. C. Saez, Neuron **6**, 305 (1991).

[15] S. O. Suadicani, M. J. Vink, and D. C. Spray, Am. J. Physiol. **279**, H3076 (2000).

[16] A. S. Lader, Y-F. Xiao, C. R. O'Riordan, A. G. Prat, G. R. Jackson, and H. F. Cantiello, Am. J. Physiol. **279**, C173 (2000).

[17] E. A. Pelleg, C. M. Hurt, and E. L. Michelson, in *Biological Actions of Extracellular ATP*, edited by G. R. Dubyak and J. S. Fedan (New York Academy of Science, New York, 1990).